Research Article

Journal of Environmental Nanotechnology

Green Functionalization of Hemp Fabrics with Pd/Pt Nanoparticles via Microwave-assisted Rose Extract Synthesis and Ridge-regularized RSM Optimization

Rekha Anantharaman[1], Lalit Chowdhury[2], Sushree Mohan[3], L. R. Sujithra[4*], A. Selvanayagi[5] and V. V. S. Sasank[6]

[1]Department of Obstetrics and Gynecology, Saveetha Medical College and Hospital, Chennai, TN, India
[2]Department of Botany, Dhenkanal Autonomous College, Dhenkanal, OD, India
[3]Department of Biology, Gwinnett Technical College, Georgia, USA, GA
[4]Department of Artificial Intelligence and Data Science, Sri Eshwar College of Engineering, Coimbatore, TN, India
[5]Department of Computer Science and Engineering, M. Kumarasamy College of Engineering, Karur, TN, India
[6]Department of Computer Science Engineering, Koneru Lakshmaiah Education Foundation, Guntur, AP, India
Received: 22.04.2026 Accepted: 29.05.2026 Published: 30.06.2026
*lrsujithra9@gmail.com

ABSTRACT

The present study investigates the sustainable functionalization of hemp fabrics through the green synthesis of Pd/Pt nanoparticles using rose petal (RPE) and rose stamen (RSE) extracts via a microwave-assisted phyto-reduction process. The successful formation and deposition of nanoparticles on the fabric surface were confirmed by UV–Vis, FTIR, DLS, XRD, and FESEM–EDX analyses, revealing an average particle size of 14.8 nm. A Ridge-regularized response surface methodology (RSM) model was developed to predict color strength (K/S) based on RPE, RSE, Pt, and Pd concentrations. The model exhibited excellent fitting performance ($R^2 = 0.9951$, RMSE = 0.0629, and MAE = 0.0473), while leave-one-out cross-validation produced an R^2 of 0.6681, indicating acceptable but moderate predictive robustness for unseen data. The optimized conditions were determined as 1.50 g RPE, 1.50 g RSE, 2.00 mM Pt, and 2.00 mM Pd, yielding a predicted K/S value of 6.6563. Compared with untreated extracts, the Pd/Pt-treated fabrics showed a marked improvement in color strength (K/S = 5.42), enhanced color fastness ratings (7–9), and strong antibacterial activity against *S. aureus* (20 mm) and *E. coli* (18 mm). These findings demonstrate that the combination of green nanoparticle synthesis and Ridge–RSM optimization provides an environmentally sustainable strategy for producing multifunctional textile materials with improved coloration and antibacterial performance.

Keywords: Photo reduction process; Antibacterial activity; Optimization; Response surface methodology; Sustainability.

1. INTRODUCTION

Recent advancements in sustainable material science have emphasized the utilization of biomass-derived resources and eco-friendly processing techniques for environmental, textile and Biomedical applications. Hemp-based materials have demonstrated excellent performance in adsorption and purification processes, where hemp and hemp biochar achieved high Cr (VI) removal efficiencies of 97.9–99.17% under optimized RSM conditions, following the Freundlich isotherm and pseudo-first-order kinetics, while ANN models accurately predicted system behavior (ul-Ain *et al.* 2025). Similarly, diamidoxime-functionalized hemp cellulose exhibited a high adsorption capacity of 220 mg/g for U(VI), supported by strong intermolecular interactions and pseudo-second-order kinetics (Kaur *et al.* 2021). In addition, DES-treated hemp fibers produced high-purity cellulose with improved crystallinity and reduced particle size (8.4–39.5 µm), achieving yields of 78–91% and solvent recovery exceeding 92%, demonstrating scalability (Haque *et al.* 2026). Furthermore, anthocyanin-loaded hemp foam exhibited rapid pH-responsive color change (pH 2–10) with 60% faster response and strong ammonia sensing capability up to 250 ppm, confirming its applicability in smart materials (Zhu *et al.* 2023).

In the field of nanomaterials and advanced composites, significant progress has been achieved using green synthesis approaches. PdPt–ZrO_2/MWCNT nanohybrids demonstrated approximately 200-fold enhancement in electrocatalytic activity due to synergistic effects and improved surface characteristics (Dabirifar *et al.* 2022). Similarly, Mn–Fe_3O_4/zeolite catalysts achieved up to 92.5% color removal and 87.6% COD removal in textile wastewater treatment, with hydroxyl radicals dominating degradation mechanisms and stable reuse performance (Özgüven *et al.* 2025). EDTA-functionalized Fe_3O_4/cocoa pod carbon composites exhibited high adsorption capacities (147.43–162.25 mg/g) following the Freundlich isotherm and pseudo-second-order kinetics, demonstrating cost-effective and recyclable performance (Thomas *et al.* 2021). Green-synthesized CuO/NG nanocomposites showed a high CO_2 adsorption capacity of 4.21 mmol/g with 93% retention after multiple cycles, indicating excellent stability (Haskan *et al.* 2025). Moreover, hemp cellulose-derived nanocomposites synthesized via pyrolysis exhibited enhanced graphitization and mesoporous structures with embedded Ni/Co nanoparticles (Bazanov *et al.* 2025).

Considerable developments have also been reported in textile dyeing and functionalization using sustainable approaches. Supercritical CO_2 dyeing with madder on polyester demonstrated eco-friendly performance, where ANN and ANFIS models effectively predicted color strength with high accuracy (<3% error) (Haji *et al.* 2025). Oxygen plasma treatment improved wool dyeing with grape leaf extract, achieving enhanced color strength with ANFIS models (R^2 = 0.997) outperforming ANN (R^2 = 0.986) (Haji and Payvandy, 2020). Similarly, ANN–GA optimization significantly improved dyeing performance, achieving K/S values of 10.21 for polyamide and 7.65 for wool, demonstrating the effectiveness of hybrid AI-based optimization (Shahmoradi *et al.* 2024). Pistachio peel extract-assisted Ag nanoparticles enhanced cotton dyeing, increasing K/S values from 3.08 to 16.07 while achieving 100% antibacterial activity and excellent durability (Sadeghi-Kiakhani *et al.* 2025b). Nanoparticle-functionalized textiles have shown remarkable improvements in multifunctional properties. Similarly, SPI-assisted ZnO nanoparticle-coated hemp fabrics achieved excellent antibacterial efficiency (99.99%) and UV protection (UPF 50+), confirming their suitability for advanced textile applications (Klaykruayat *et al.* 2026). Ag nanoparticle-treated hemp fabrics exhibited strong antibacterial durability exceeding 90% even after 30 washing cycles, along with improved thermal stability (Sasunthon *et al.* 2025).

Advanced modeling and optimization techniques have further enhanced the efficiency and predictability of material processing systems. PSO-ANN hybrid models achieved extremely high prediction accuracy ($R^2 \approx 0.999$) in activated carbon production (Orero *et al.* 2025). ANN-based models consistently outperformed conventional RSM approaches with reduced error margins in wastewater treatment systems (Patel *et al.* 2026). Hybrid BOA-BRT models demonstrated superior predictive capability compared to ANN, SVR, and RSM for microplastic removal, highlighting the importance of advanced machine learning approaches (Hossain, 2025). Additionally, ANN–GA and ANFIS-based models have proven highly effective in optimizing dyeing processes with high accuracy and reduced experimental effort (Shokrzadeh *et al.* 2025).

This work introduces a novel approach for hemp textile functionalization by combining rose waste-derived Pd/Pt bimetallic nanoparticle synthesis with Ridge-regularized response surface methodology. The study uniquely integrates sustainable biomass utilization and regularized predictive modeling to optimize color strength while simultaneously enhancing durability and antibacterial activity, providing a scalable framework for multifunctional textile development.

This study presents a novel integration of green phytosynthesis and advanced statistical modeling for the functionalization of hemp textiles using Pd/Pt bimetallic nanoparticles derived from rose waste extracts. Unlike conventional approaches, a Ridge-regularized response surface methodology (RSM) is employed to enhance predictive stability and address multicollinearity issues inherent in nonlinear systems. The work uniquely combines sustainable biomass utilization with regularized modeling to establish a robust framework for optimizing colorimetric performance. Furthermore, the synergistic interaction between phytochemicals and bimetallic nanoparticles enables simultaneous improvement in color strength, durability, and antibacterial functionality. This integrated approach provides a sustainable and scalable pathway for the development of multifunctional textile materials.

2. MATERIALS AND METHODOLOGY

Rose petals and stamens obtained from the local market in Erode, Tamil Nadu, India, were shade-dried and ground into a consistent fine powder. To ensure consistency, rose remnants were sourced from a single vendor, and the synthesis process was executed three times under identical conditions, guaranteeing reproducibility. The sieved powder was later employed for extraction and coloring tests. The research utilized plain-woven hemp fabric (pre-scoured, 16 wefts/cm and 12 warps/cm) sourced from Fiber Source Enterprises, Chennai. Analytical-grade hexachloroplatinic acid hexahydrate ($H_2PtCl_6 \cdot 6H_2O$, ≥99%) and palladium acetate ($Pd(CH_3COO)_2$, ≥99%) were obtained from Star Scientific Enterprises, Erode, Tamil Nadu, India.

2.1 Preparation of RPE and RSE

To prepare RPE and RSE, the rose material was thoroughly shade-dried and finely pulverized with a mechanical grinder to get a uniform consistency. For extraction, different quantities of powdered petals and stamens were combined with 70 mL of DI water. The combinations underwent microwave-assisted extraction at different power levels (60, 80, and 100 W) for periods of 5, 10, and 15 minutes. Subsequent to irradiation, solutions was let to cool spontaneously to room temperature. These were filtered with filter paper to eliminate contaminants and kept at 5 °C for subsequent experimental use.

2.2 Photosynthesis of Pd/Pt NPs at Hemp

Synthesis technique with the formulation of aqueous solutions including Pd and Pt salts at concentrations of 0.5, 1, 1.5, and 2 mM. The plant extracts were subsequently amalgamated with the metal precursor solutions in diverse ratios and concentrations, resulting at establishment of 50 experimental conditions. The notable color change was seen at reaction mixture upon the combination of metal ion solutions with the extracts at mild heating and constant agitation. Similarly, saffron petal extracts enabled the phytosynthesis of Pd nanoparticles (~31 nm) on wool, confirmed by FTIR, SEM, and DLS analyses. PdNP incorporation enhanced antibacterial activity (up to 100%) with good colorfastness, offering a sustainable textile finishing approach (Sadeghi-Kiakhani *et al.* 2025a).

For dyeing preparation, 1 g samples of hemp fibers were first purified using 0.5% non-ionic detergent at 55 °C for 30 minutes, with a liquor-to-material ratio of 40:1. Sample was subsequently rinsed in DI water to eliminate leftover detergent and air-dried under ambient conditions. Subsequent to pretreatment, each of the 50 experimental solutions was administered to the samples individually at a liquid-to-gas ratio of 50:1. The dyeing was conducted under optimal microwave settings at 80 W for 15 minutes. Thereafter, treated materials were rinsed with DI water to remove unbound dye and dried at oven on 40 °C. All dyeing experiments were performed under identical conditions, and the reported K/S values represent the mean of repeated measurements**.** The color characteristics of dyed fabrics were quantitatively assessed by reflectance spectrophotometry, emphasizing K/S values derived from the Kubelka–Munk equation (Safi and Amirshahi, 2023).

Fig. 1: Microwave-assisted Pd/Pt phytosynthesis of nanoparticles

2.3 Analysis Methods

The extraction of natural pigments from petals and stamens was performed using the Microwave Milestone flexiWAVE device. The optical properties of Pd/Pt nanoparticles synthesized with the extracts were analyzed using a Shimadzu double-beam UV–Vis spectrophotometer. Chemical characterisation of Pd/Pt-coated hemp fibers was performed using several methods. Functional groups were analyzed using FTIR spectroscopy (Nicolet Nexus 670, USA) within the range of 400–4000 cm^{-1}. The elemental composition and surface morphology was examined with FESEM coupled by EDX (Zeiss Gemini). The particle size were analysed using Dynamic Light Scattering (DLS). In previous research, hemp-derived lignin nanoparticles were functionalized via DES and amination, with Dynamic Light analysis confirming particle size increase and enhanced adsorption (Rakphong *et al.* 2025). Crystalline structure were analyzed using X-ray diffraction (XRD) with Bruker throughout a 2θ range of 10°–80°, and the elemental composition was confirmed using X-ray fluorescence (XRF) with the same apparatus. Color characteristics, including CIELAB and K/S values, were measured by an X-Rite 7000 A spectrophotometer.

Chroma (C), denoting color intensity and were computed by Equation (1):

$$C^* = \left(a^{*2} + b^{*2}\right)^{\frac{1}{2}} \qquad \ldots (1)$$

The color strength parameter (C), indicating color saturation, was computed using Equation (1):

$$h^\circ = \tan^{-1}\left(\frac{b^*}{a^*}\right) \qquad \ldots (2)$$

a* and b* represent color coordinates at CIELAB system.

The color depth was evaluated by the Kubelka–Munk equation, which relates scattering (S) and absorption (K) coefficients to reflectance (R) as expressed in Eqn. (3):

$$\frac{K}{S} = \frac{(1-R)^2}{2R} \qquad \ldots (3)$$

2.4 Statistical Modeling and Analysis

To improve the predictive capability of the conventional RSM model, Ridge regression was incorporated into the quadratic response surface framework. Initially, second-order polynomial features were generated from the input variables (RPE, RSE, Pt, and Pd), including linear, interaction, and squared terms. Subsequently, Ridge regularization was applied to the regression model to penalize large coefficient values and reduce multicollinearity effects. This hybrid Ridge–RSM approach enhances model stability and improves prediction accuracy for nonlinear systems (Table 1). Earlier investigation indicates that the cellulase pretreatment optimized using RSM, Polynomial modeling, and Ridge analysis significantly enhanced fiberboard bending strength to 25.12 MPa (Wu *et al.* 2020).

Table 1. ANN model parameters for K/S prediction

Model Parameter	Specification
Model Type	Feedforward Neural Network (FNN)
Input	RPE (g), RSE (g), Pd (mM), Pt (mM)
Output	Color Strength (K/S)
Number of Hidden Layers	2
Neurons per Layer	8 (Layer 1), 4 (Layer 2)
Learning Rate	0.01
Optimizer	Adam
Loss Function	Huber Loss
Activation Function (Output)	Linear
Activation Function (Hidden)	Tanh
Regularization	L2 ($\lambda = 1 \times 10^{-4}$)
Data Normalization	StandardScaler (Z-score normalization)
Batch Size	8
Epochs	200
Validation Strategy	LOOCV (Leave-One-Out Cross Validation)

The ANN model was configured to capture nonlinear relationships between process parameters and K/S response. A two-hidden-layer architecture with 8 and 4 neurons was employed to balance model complexity and generalization. Tanh activation was used in hidden layers, while a linear activation function was adopted at the output layer for regression. The model was trained by the Adam optimizer with Huber loss to ensure robustness against outliers. To evaluate predictive performance and assess overfitting, leave-one-out cross-validation (LOOCV) was applied. The ANN model was employed as a supplementary predictive tool to benchmark the performance of the proposed Ridge-RSM approach. However, Ridge-RSM remained the primary framework for process optimization owing to its greater interpretability and ability to address multicollinearity among process variables.

2.5 Analysis of Colorfastness

Lightfastness of samples was evaluated according to ISO 105 B02:1994 using a SOLARBOX weathering machine for light exposure. Color retention was analysed by contrasting exposed and unexposed regions with blue wool standards. Washfastness testing was conducted following ISO 105-C10:2006 (E), assessing stains using standardized grayscale ratings. The rubbing fastness was evaluated using a crockmeter (ISO 105-X12:1993 (E)) in damp and dry conditions with fixed hemp samples subjected to ten rubbing cycles, and color transfer to adjacent white cloth was assessed through grayscale analysis. Previous studies have reported that, the dyed fabrics showed excellent colorfastness and UV protection (UPF > 40), highlighting sustainable textile applications (Klaykruayat *et al.* 2024).

2.6 Antibacterial Activity Measurement

Antibacterial experiments were performed on two sample sets: fabrics treated with RPE/RSE and Pd/Pt ions, and untreated hemp material. To avert contamination, all hemp specimens, containers, and devices were subjected to UV sterilization before inspection. This procedure verified that any observed antibacterial effect was solely due to the treated materials.

Standard bacterial suspensions were made by adding 8 mL of sterile LB broth to microvials with cultures of Gram-positive Staphylococcus aureus and Gram-negative Escherichia coli. Cultures were incubated at 36 °C for 20 hours to reach the late logarithmic phase, thereby ensuring vigorous microbial populations for evaluation. Antibacterial efficiency was evaluated using optical density measurements with a spectrophotometer, reflecting bacterial concentration by light absorbance. Variations in optical density measurements were employed to evaluate growth inhibition and bacterial reduction. The antibacterial performance of treated hemp fabrics was assessed by the standard equation (Eq. 4) and analysed per the AATCC 100 technique by comparing colony-forming units (CFU/mL) among untreated control samples and treated samples containing RPE/RSE and Pd/Pt nanoparticles (Test). Reduced CFU levels in treated samples indicated effective antibacterial activity. According to the prior study, hemp leaf extracts enabled green synthesis of stable spherical AgNPs with strong antioxidant and antibacterial activity (Csakvari *et al.* 2021).

$$\text{Antibacterial activity } (\%) = \frac{\text{Blank} - \text{Test}}{\text{Blank}} \times 10 \quad \dots (4)$$

3. RESULTS AND DISCUSSION

3.1 RPE/RSE-mediated Pd/Pt NP Synthesis

UV–Visible spectroscopy is an effective technique for evaluating spectral properties and quantifying solution concentration in diverse systems. It was also utilized to verify the synthesis of Pd/Pt bimetallic nanoparticles produced by RPE/RSE (Fig.3b). Previous research has recorded the synthesis of Pd nanoparticles using RPE and RSE, along with a thorough analysis. UV–Visible spectra of RPE/RSE displayed a prominent absorption peak at around λ_{max} = 230 nm, linked to flavonoids and polyphenolic chemicals. These biomolecules possess inherent redox activity, enabling interaction with metal ions and regulating nucleation without external stabilizers. Functional compounds, such as carbonyl and carboxyl moieties, along with aromatic rings in polyphenols, facilitated redox reactions that converted ions into Pd/Pt nanoparticles (Figure 3a). The injection of Pt^{2+} and Pd^{2+} ions into RPE/RSE caused a noticeable color change, signifying nanoparticle formation, which was later validated by UV–Visible analysis. Unlike monometallic noble metal nanoparticles that often exhibit distinct localized surface plasmon resonance (LSPR) bands, Pd and Pt nanoparticles generally display broad and less pronounced absorption features due to strong interband electronic transitions and damping effects. In the present study, the broad absorption profile observed after metal ion reduction indicates the successful formation of nanoscale Pd/Pt bimetallic particles. Furthermore, the interaction between Pd and Pt atoms can alter the electronic structure and surface charge distribution, resulting in modified optical behavior compared with their individual counterparts. The absence of additional absorption bands suggests the formation of well-dispersed nanoparticles with minimal aggregation, which is consistent with the DLS, XRD, and FESEM observations. This study employed techniques to enhance extraction parameters and examine the absorption properties of the specimen (Figure 2). The findings indicate that RPE/RSE function as superior stabilizing and reducing agents for the manufacture of homogeneous Pd/Pt nanoparticles without chemical additions.

FTIR analysis was performed to identify the functional groups involved in the reduction and stabilization of Pd/Pt nanoparticles. As shown in Fig. 3(c), the spectra of RSE, RPE, and RPE/RSE exhibited a broad band around 3300 cm⁻¹ corresponding to phenolic –OH groups, while peaks at 2947, 1483, 1289, and 941 cm⁻¹ were attributed to C–H, C=C, C–O, and ester carbonyl vibrations, respectively. Compared with the plant extracts, the Pd/Pt-containing sample showed a decrease in the intensity of the band at 1768 cm⁻¹ and the appearance of a new peak at 588 cm⁻¹, confirming the involvement of phytochemical functional groups in the formation and stabilization of Pd/Pt nanoparticles.

DLS analysis was used to assess particle size of Pd/Pt generated by RPE/RSE. Figure 3d illustrates that the average particle diameter was around 14.8 nm, which is within the conventional nanoscale of less than 30 nm, thereby validating the successful creation of nanoparticles. A polydispersity index (PDI) of 0.18 indicates a relatively narrow particle size distribution and good dispersion uniformity of the synthesized nanoparticles. However, PDI primarily reflects size homogeneity and does not independently confirm long-term colloidal stability. Nevertheless, the low PDI value suggests limited aggregation and effective phytochemical stabilization of the Pd/Pt nanoparticles.

3.2 Statistical Modeling and Validation (Ridge-RSM)

Table 2 shows the Ridge-regularized RSM model demonstrated high training performance with a coefficient of determination (R^2 = 0.9951), along with low error values (MSE = 0.00396, RMSE = 0.06293, and MAE = 0.04731), indicating strong agreement between predicted and experimental data. However, the LOOCV results revealed variability in predictive performance, with a mean CV R^2 of −2.9229 and a wide dispersion across folds. The overall CV R^2 of 0.6681 suggests acceptable but moderate generalization capability under unseen conditions. These findings indicate that, although the model effectively captures the experimental trends, its predictive stability across validation folds is limited. The incorporation of Ridge regularization contributes to improved coefficient stability and reduced sensitivity to multicollinearity. Therefore, further experimental validation is recommended to confirm the robustness of the predicted optimal conditions. The significant improvement in R^2 compared to the conventional RSM model ($R^2 \approx 0.75$) can be attributed to the incorporation of Ridge regularization, which effectively stabilizes coefficient estimation and mitigates multicollinearity among polynomial terms.

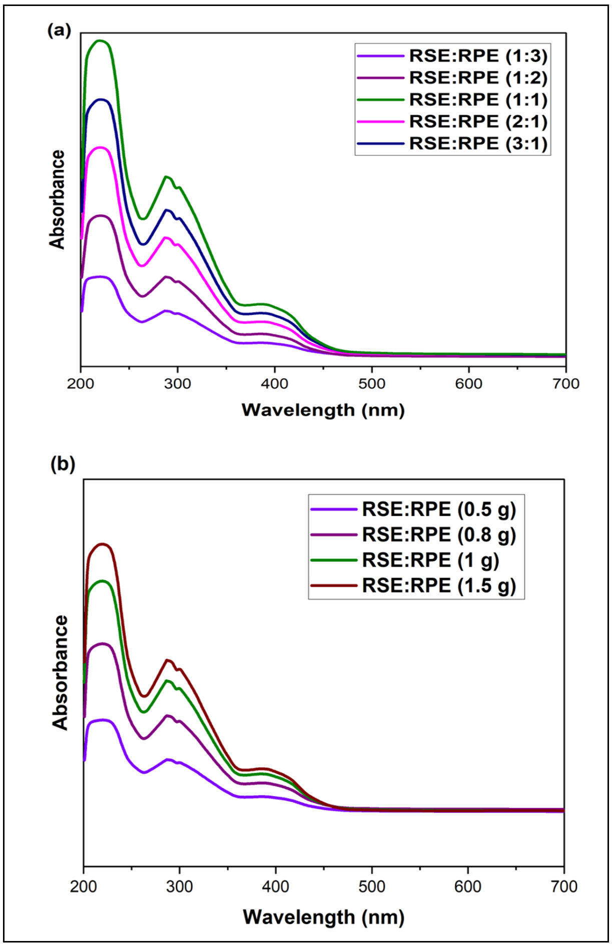

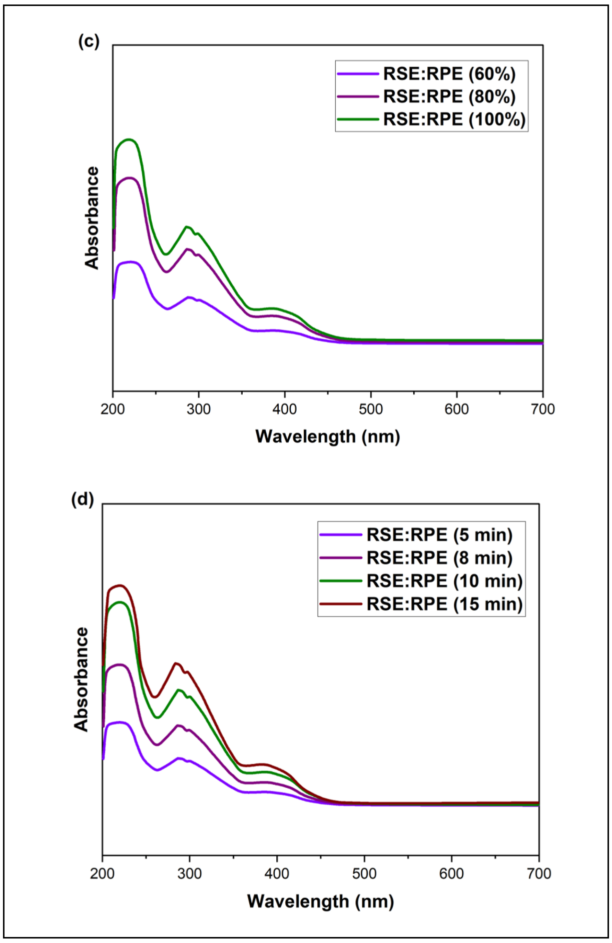

Fig. 2: Optimization of (a) the RSE/RPE ratio in the formulation, (b) the amount of plant material in 70 mL of water, (c) microwave power and (d) microwave extraction time for the extraction process of RS/RP

Based on the regression coefficients, a second-order polynomial model was formulated to predict the color strength (K/S) of bimetallic Pd/Pt nanoparticle-coated hemp fibers as a function of the processing variables (RPE, RSE, Pt, and Pd). The developed equation incorporates linear, interaction, and quadratic terms, enabling a comprehensive evaluation of factor contributions. The positive coefficients of the linear terms (RPE, RSE, Pt, and Pd) indicate that increasing these parameters initially enhances the color strength due to improved nanoparticle formation and deposition on the fiber surface. Significant interaction terms, particularly RPE×RSE, RPE × Pd, and Pt × Pd, highlight synergistic effects between plant extracts and metal precursors, contributing to enhanced coloration efficiency. Conversely, the negative coefficients of the quadratic terms (RPE^2, RSE^2, Pt^2, and Pd^2) confirm the existence of an optimum region, beyond which further increases in factor levels lead to a decline in K/S values, likely due to saturation effects and nanoparticle agglomeration. Overall, the model effectively captures the nonlinear behavior of the system and provides a useful framework for optimizing color strength within the investigated experimental domain. However, the LOOCV results indicate moderate predictive robustness, suggesting that further validation with larger datasets would be beneficial. In addition, gromwell-derived natural dyes exhibited strong colorfastness, antioxidant, and antibacterial properties, supporting eco-friendly textile innovations.

$$K/S = -0.159 + 1.660(RPE) + 1.589(RSE) + 0.824(Pt) + 0.512(Pd) - 1.466(RPE2) + 1.163(RPE \cdot RSE) + 0.063(RPE \cdot Pt) + 0.971(RPE \cdot Pd) - 1.100(RSE2) + 0.821(RSE \cdot Pt) - 0.391(RSE \cdot Pd) - 0.711(Pt2) + 0.860(Pt \cdot Pd) - 0.619(Pd2)$$

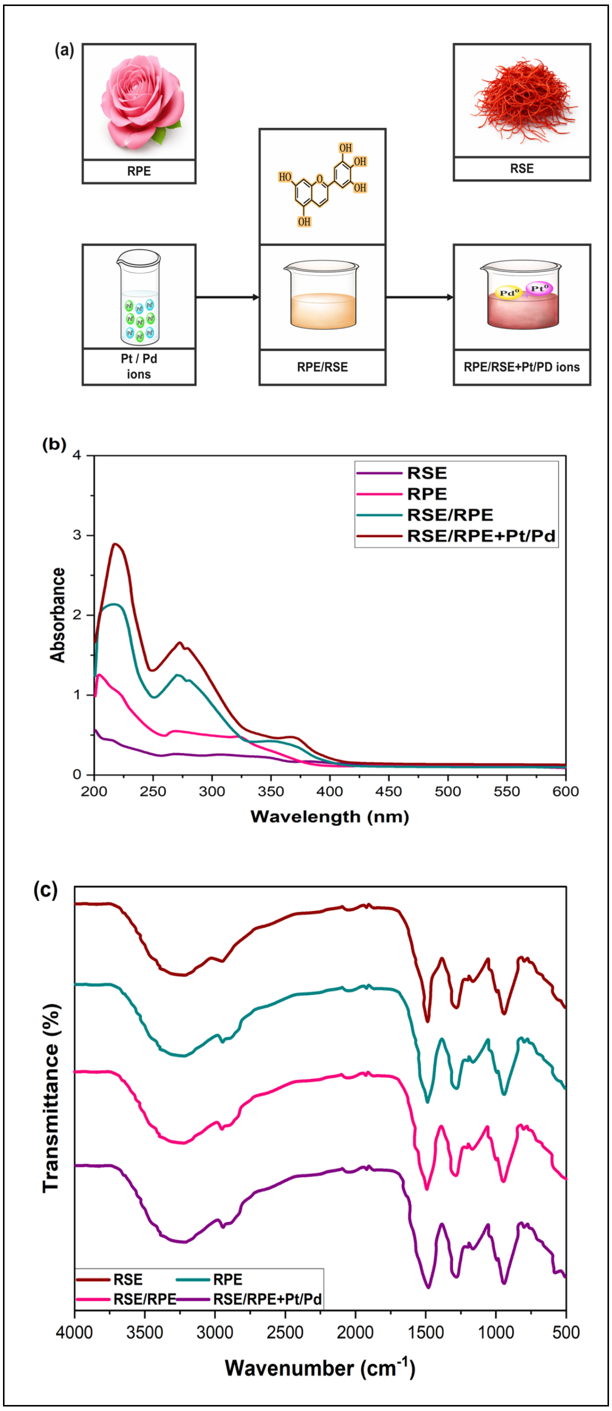

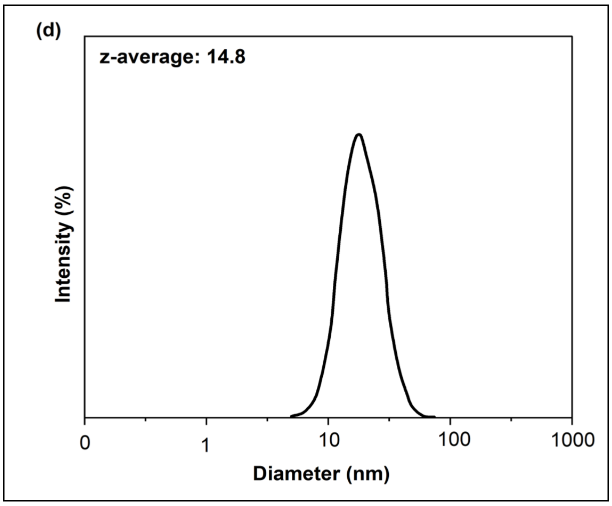

Fig. 3: (a) Flavonoid-mediated Pd/Pt redox mechanism (b) UV–vis spectra of RPE/RSE systems (c) FTIR spectra of extract–metal systems and (d) DLS analysis of Pd/Pt NPs

Table 2. Statistical metrics

Metric	Value
R^2	0.995134
MSE	0.00396
RMSE	0.062926
MAE	0.047309
CV R^2 (Mean)	-2.92286
CV R^2 (Standard Deviation)	6.599131
CV R^2 (Minimum)	-16.085
CV R^2 (Maximum)	0.869616
CV Mean Square Error (Mean)	0.270066
CV Mean Square Error (Standard Deviation)	0.239551
CV RMSE (Mean)	0.477349
CV RMSE (Standard Deviation)	0.205435
CV Mean Absolute Error (Mean)	0.379104
CV Mean Absolute Error (Standard Deviation)	0.12675
CV R^2 (Overall)	0.668099

3.3 Response Surface Analysis (RSM Coefficients)

The regression coefficients of the developed quadratic RSM model (Table 3) quantitatively describe the influence of linear, interaction, and quadratic terms on the color strength (K/S) of Pd/Pt nanoparticle-coated hemp fibers. The linear terms for RPE (1.6603) and RSE (1.5891) exhibit the highest positive contributions, confirming that plant extracts play a dominant role in nanoparticle reduction and subsequent enhancement of fiber coloration, while Pt (0.8235) and Pd (0.5115) also contribute positively to K/S. Significant interaction effects, particularly RPE × RSE (1.1629), RPE × Pd (0.9712), and Pt × Pd (0.860), indicate strong synergistic behavior between phytochemicals and bimetallic precursors, promoting effective nucleation and uniform nanoparticle deposition within the fiber matrix. In contrast, the negative quadratic coefficients for RPE^2 (−1.4665), RSE^2 (−1.100), Pt^2 (−0.711), and Pd^2 (−0.619) confirm the existence of an optimal region, beyond which excessive factor levels lead to reduced K/S due to saturation and possible nanoparticle agglomeration. Overall, the coefficient trends highlight the nonlinear and interactive nature of the system, validating the capability of the developed model to accurately represent and optimize the green synthesis process for sustainable textile functionalization. Recent studies demonstrate that henna-based dyeing of hemp in $scCO_2$ achieved optimal color strength at 120 °C, 21 MPa, and 90 min using RSM optimization. Waterless dyeing showed good model accuracy and sustainable performance, offering an eco-friendly alternative to conventional methods (Eren *et al.* 2025).

Table 3. Coefficients

Term	Coefficient
Intercept	-0.15926
RPE	1.660294
RSE	1.589118
Pt	0.8235
Pd	0.5115
RPE^2	-1.46647
RPE × RSE	1.162941
RPE × Pt	0.063176
RPE × Pd	0.971176
RSE^2	-1.1
RSE × Pt	0.821176
RSE × Pd	-0.39082
Pt^2	-0.711
Pt × Pd	0.86
Pd^2	-0.619

The response surface plots shown in Figure 4 illustrate the interactive effects of RPE, RSE, Pt ions, and Pd ions on the K/S response of hemp fabric. In general, the surfaces exhibit a gradual increase in K/S values with increasing concentrations of both plant extracts and metal ions, confirming their positive influence on color strength. The combined effect of RPE and RSE demonstrates a pronounced curvature, indicating strong interaction and the presence of an optimal region at higher extract concentrations. Similarly, the interaction between Pt and Pd ions shows a synergistic enhancement of the response, where higher levels of both ions contribute to improved K/S values. The contour projections further support these observations, revealing nonlinear relationships and interaction dominance among the variables. The peak regions observed in the plots correspond to the upper levels of RPE, RSE, Pt, and Pd, validating the optimization results and confirming that maximum color strength is achieved through the combined effect of extract concentration and bimetallic ion interaction.

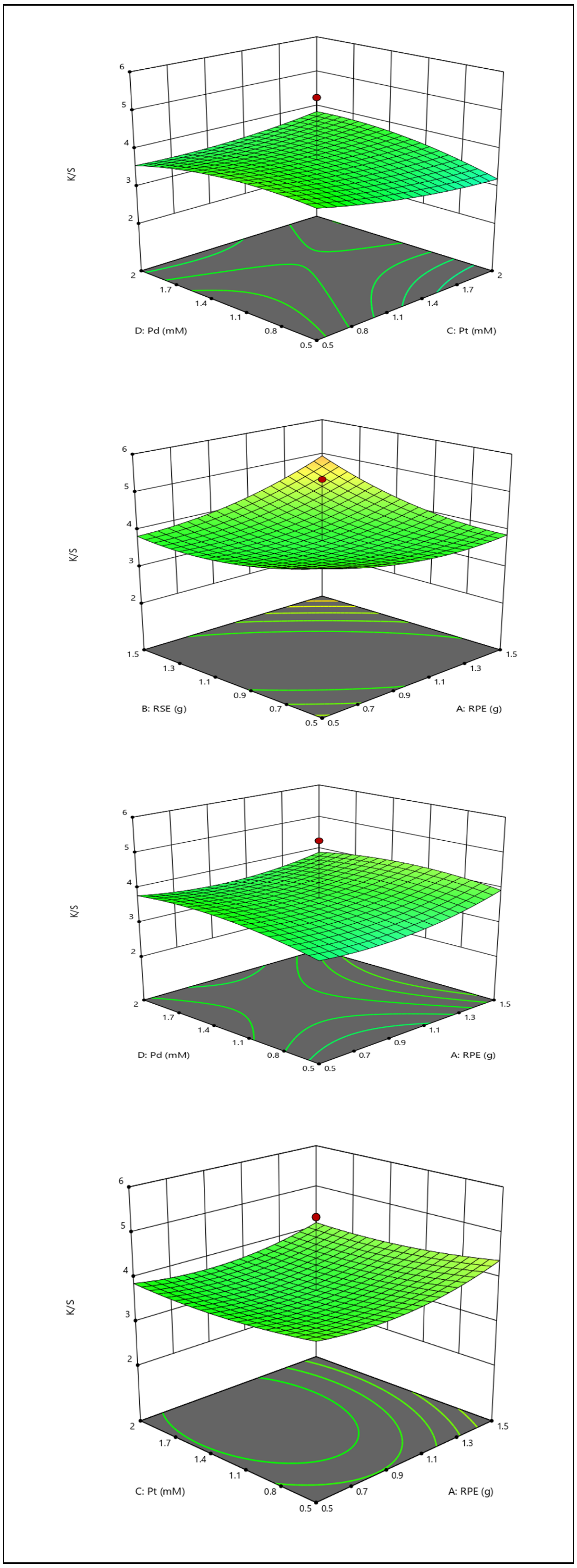

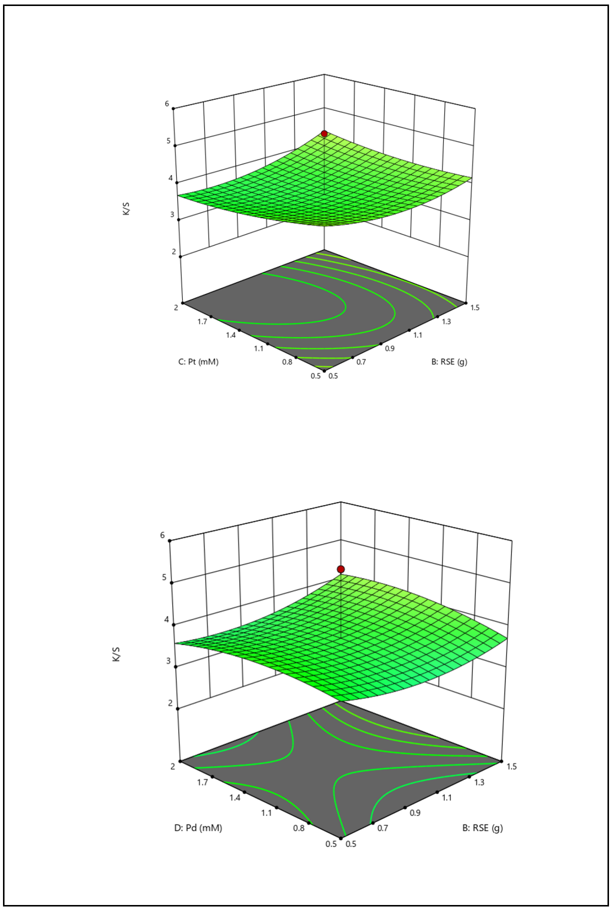

Fig. 4: Response surface plots showing interaction of RPE, RSE, Pt ions, and Pd ions on the K/S response

3.4 Process Optimization and Validation

The Ridge–RSM optimization approach was applied to determine the optimal dyeing conditions for maximizing color strength (K/S) of hemp fibers (Figure 5). The model predicted an optimum combination of 1.50 g RPE, 1.50 g RSE, 2.00 mM Pt, and 2.00 mM Pd, corresponding to a predicted K/S value of 6.6563, indicating an improvement over the initial experimental conditions. The predictive performance of the model was evaluated using diagnostic plots. The Actual vs. Predicted plot provides strong linear correlation, with data points closely aligned with the 45° reference line, indicating good agreement between experimental and fitted values. Similarly, the Actual vs. LOOCV Predicted plot indicates moderate predictive consistency under cross-validation conditions. The residual plot exhibits a random distribution around zero, suggesting the absence of significant systematic errors and supporting the assumption of homoscedasticity. However, the variability observed in LOOCV metrics indicates that the model exhibits limited generalization stability across validation folds. Although low RMSE values were observed for the training data, the differences between training and validation performance suggest that further experimental validation is required to confirm the robustness of the predicted optimum conditions. Overall, the Ridge-regularized RSM model can be considered a useful predictive tool for process optimization, with moderate generalization capability. According to the previous analysis, RSM optimization identified padding as the best technique for myrobalan dyeing, improving color uniformity and reducing time and water use. Optimal conditions (20% owf, 50°C) ensured sustainable and efficient natural dyeing for commercial applications (Agrawal, 2025).

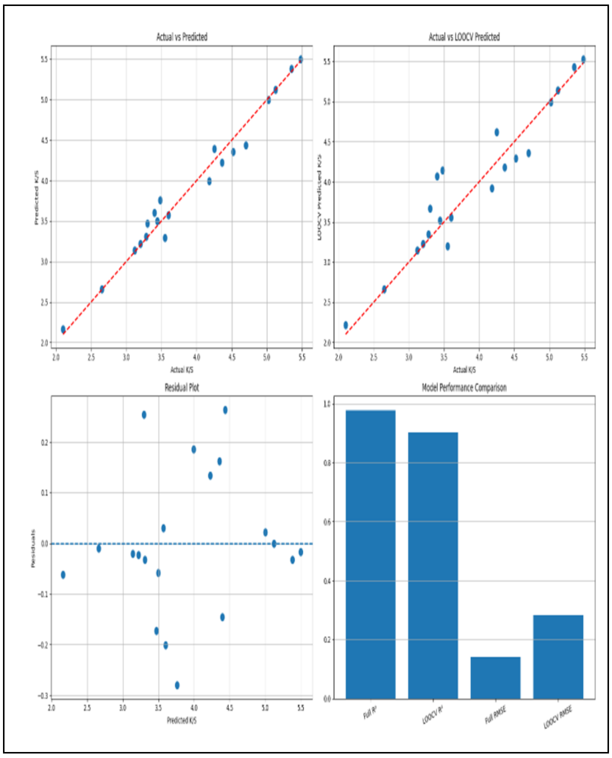

Fig. 5: Ridge–RSM model validation and performance analysis plots

3.5 Analysis of Pd/Pt NPs on Hemp

RPE/RSE were rich in bioactive chemicals, including alkaloids, polyphenols, terpenoids and flavonoids, which function as stabilizing and reducing agents in the creation of metal nanoparticles. Similarly, hymenocardia acida extracts contained diverse bioactive chemicals, including flavonoids, coumarins, terpenoids, alkaloids, polyphenols, glycosides, and disaccharides, showing strong antioxidant and antimicrobial activity (Malebo *et al.* 2026). Exposure of hemp fibers to a solution containing plant extract and metal ions promotes the reduction of metal ions, showing the in situ synthesis of nanoparticles on cellulose fibers. Deposition transpires for two primary reasons: carbonyl (C=O) groups and the existence of hydroxyl (–OH) at cellulose-binding sites for metal ions, and the capacity of plant-derived molecules to complexes with metal ions, thereby facilitating their proximity to the fiber surface and improving reduction. The stability of nanoparticles on the hemp substrate post-formation is governed by various factors.

- Nanoparticles form covalent bonds at groups cellulose (e.g., –COOH, –OH), whereas metal ions participate in interactions by negatively charged groups at fibers.
- Functional groups at plant-derived compounds and nanoparticles can establish hydrogen bonds with cellulose, improving nanoparticle bonding.

When nanoparticles and fibers surface exhibit opposite charges, electrostatic interactions facilitate bonding (Fig. 6a). The bioorganic chemicals at plant extract including polyphenols, provide protective layer around nanoparticles, improving long-term stability and minimizing aggregation by restricting oxidation.

FTIR analysis were performed to examine adhesion of Pd/Pt nanoparticles to hemp fibers utilizing RPE, RSE, and RPE/RSE. Spectra of treated fibers exhibited a significant peak at 3329cm^{-1}, signifying –OH stretching vibrations. A band at around 2863 cm^{-1} was ascribed to C–H stretching at cellulose, whereas peak at 1411 cm^{-1} were associated with CH_2 groups or C–H bending. Absorption at 1211 cm^{-1} corresponded C–O–C stretching, while band 1011 cm^{-1} was related to C–O stretching inside polysaccharide framework of cellulose. Prior work indicates that, hemp-derived cellulose nanoparticles (CNCs) reinforced nanocomposites achieved 161% tensile strength improvement at 10 wt% loading by enhanced interfacial bonding. FTIR confirmed strong hydrogen bonding with improved crystallinity and thermal stability demonstrating efficient load transfer (Aras *et al.* 2025).

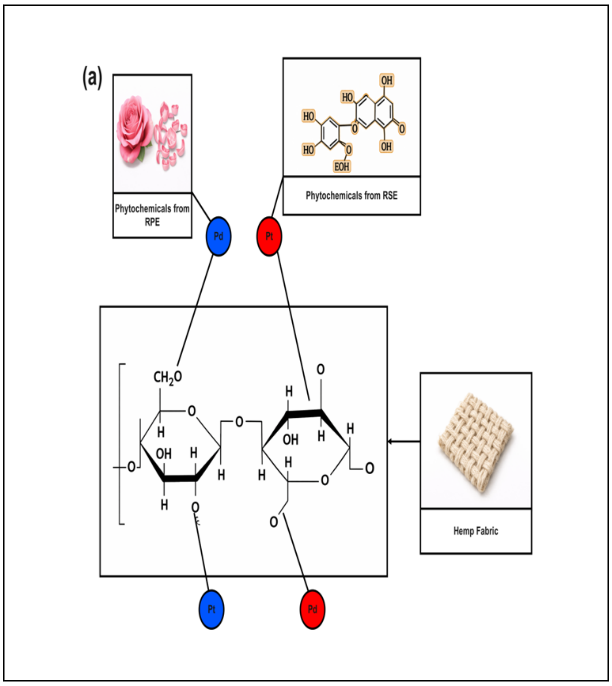

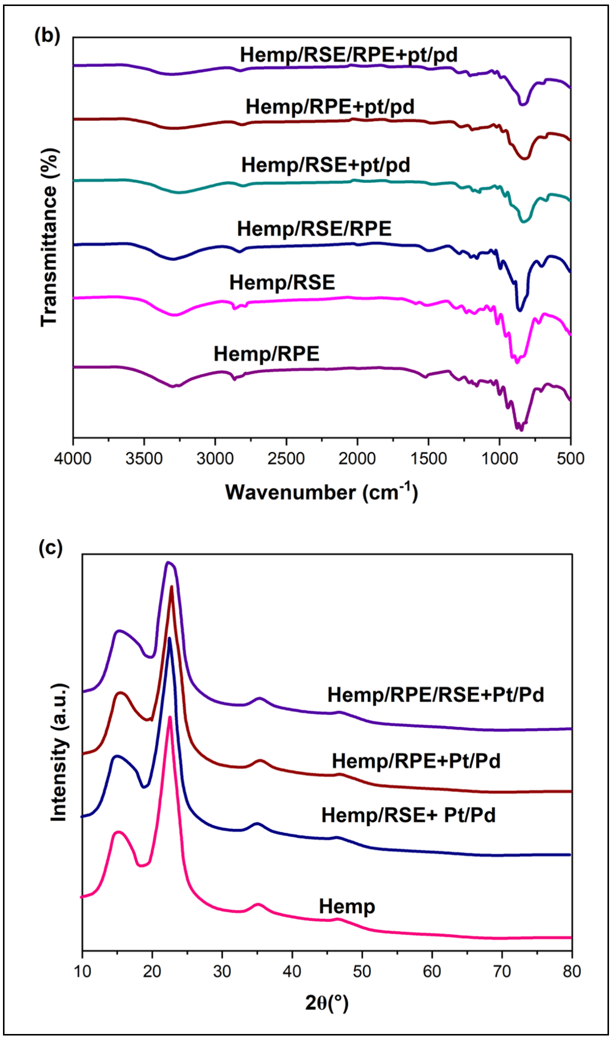

Fig. 6: (a) Interaction mechanism diagram, (b) FTIR spectral analysis and (c) XRD pattern analysis

The comparison of the RPE/RSE spectrum with the individual RPE and RSE spectra revealed improved intensity in certain locations, without the emergence of new peaks. A moderate band at 702 cm^{-1} was detected in Pd/Pt-treated fibers, regardless of the extract employed. Furthermore, fluctuations at the band at 1501 cm^{-1} signified successful integration of Pd/Pt nanoparticles on and at surface of hemp fiber.

XRD analysis was utilized to investigate the synthesis of Pd/Pt Nps at hemp fibers. Figure 6c illustrates that the diffraction pattern of untreated hemp displays peaks at 2θ values of 15.09°, 22.4°, 35.0°, and 46.6°, which correspond to the (110), (110), (200), and (004) planes of cellulose, thus affirming its crystalline structure. Following nanoparticle deposition via RSE, RPE, and RPE/RSE, supplementary peaks emerged at 2θ values of 35°, 46°, 60°, and 71°, corresponding to (111), (200), (220), and (311) planes, showing the production of Pd/Pt nanoparticles exhibiting FCC structure. Notwithstanding the integration of nanoparticles, distinctive cellulose peaks remained unaltered, indicating the retention of the crystalline structure of hemp fibers. The diffraction peaks observed at approximately 35°, 46°, 60°, and 71° can be attributed to the crystalline Pd/Pt phase and are indicative of successful nanoparticle formation on the hemp fiber surface. The appearance of these additional reflections after treatment confirms the incorporation of Pd/Pt nanoparticles, while the persistence of the characteristic cellulose peaks suggests that the native crystalline structure of the hemp fibers was preserved. Furthermore, the coexistence of cellulose and Pd/Pt diffraction peaks indicates that nanoparticle deposition occurred predominantly on the fiber surface without causing significant structural degradation of the substrate. The XRD data validate the effective synthesis and structural integrity of Pd/Pt nanoparticles on hemp. Compared to previous research, hemp fibers with Ag nanoparticles were developed by green synthesis, showing enhanced K/S, UV protection (UPF 50+), and antibacterial activity. XRD confirmed nanoparticle formation, with alkaline conditions improving multifunctional fibers performance (Chitichotpanya *et al.* 2026).

The SEM micrographs illustrate the progressive variation in surface morphology and structural features of the fiber as depicted in Fig.7 (a–d). In Fig. 7 (a), the fiber surface appears relatively compact with distinct longitudinal grooves and layered structures, accompanied by minor surface irregularities and micro voids, indicating the presence of natural impurities and weak interfacial characteristics. In Fig.7(b), the morphology exhibits increased surface roughness with the appearance of microcracks, fibrillar splitting, and localized pits, suggesting the initiation of surface degradation and partial removal of amorphous constituents such as hemicellulose and lignin. A more pronounced fibrillation is observed in Fig.7 (c), where the outer layer shows peeling and fragmentation, exposing internal microfibrils and enhancing the surface texture, which contributes to improved mechanical interlocking potential. Finally, Fig.7 (d) demonstrates a highly roughened and heterogeneous surface with evident fibril separation, debris deposition, and irregular topography, indicating significant structural modification and increased surface area. The overall morphological evolution from Fig. 7 (a) to Fig. 7 (d) confirms the transition from a relatively smooth and impurity-covered surface to a more fibrillated and roughened structure, which promotes improved nanoparticle deposition and retention on the fiber surface, thereby enhancing the functional properties of the treated textile. The increased surface roughness and fibrillated morphology observed after treatment are expected to provide additional active sites for Pd/Pt nanoparticle anchoring, thereby enhancing nanoparticle retention on the fiber surface. This improved surface interaction is consistent with the observed increase in color strength (K/S), color fastness, and antibacterial performance of the treated hemp fabrics. A prior study indicates that an acid-functionalized Moringa oleifera biosorbent achieved 99.81% Titan Yellow removal, with SEM confirming a porous structure and effective dye uptake. ANN ($R^2 = 0.998$) and RSM-BBD optimization validated high efficiency, following Langmuir isotherm and pseudo-second-order kinetics (Nayak *et al.* 2025).

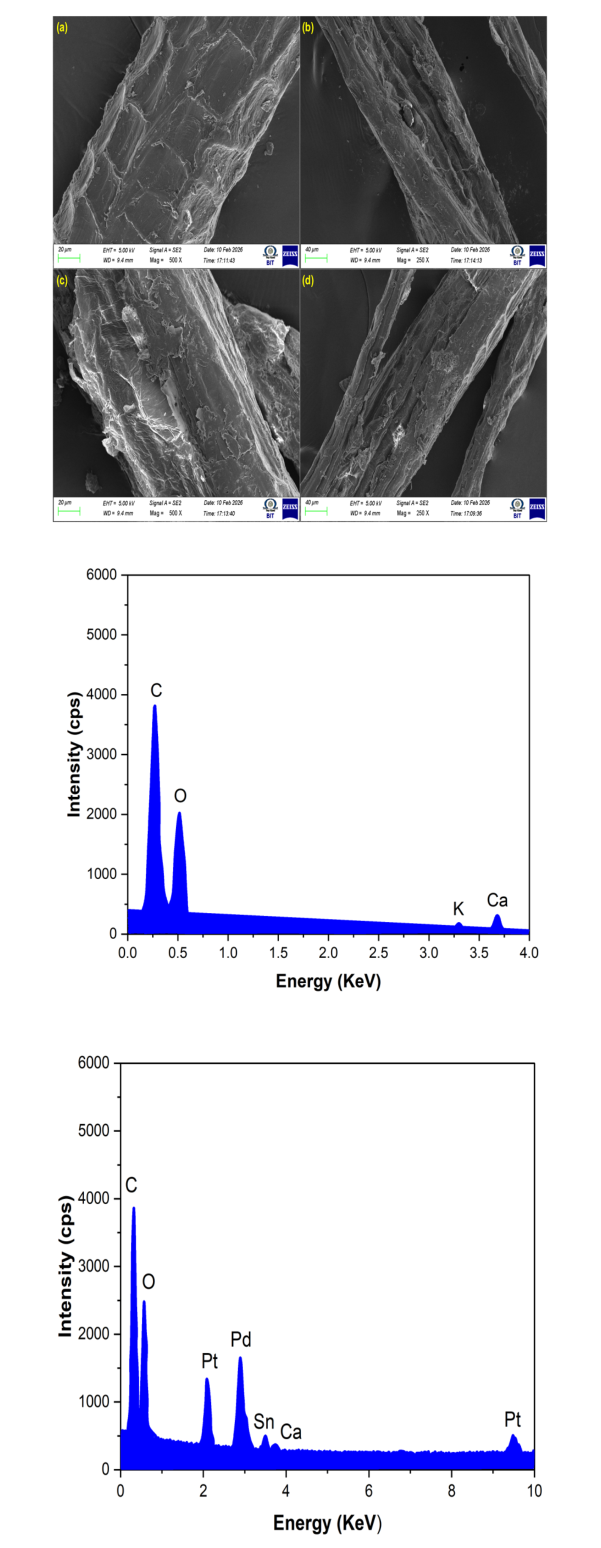

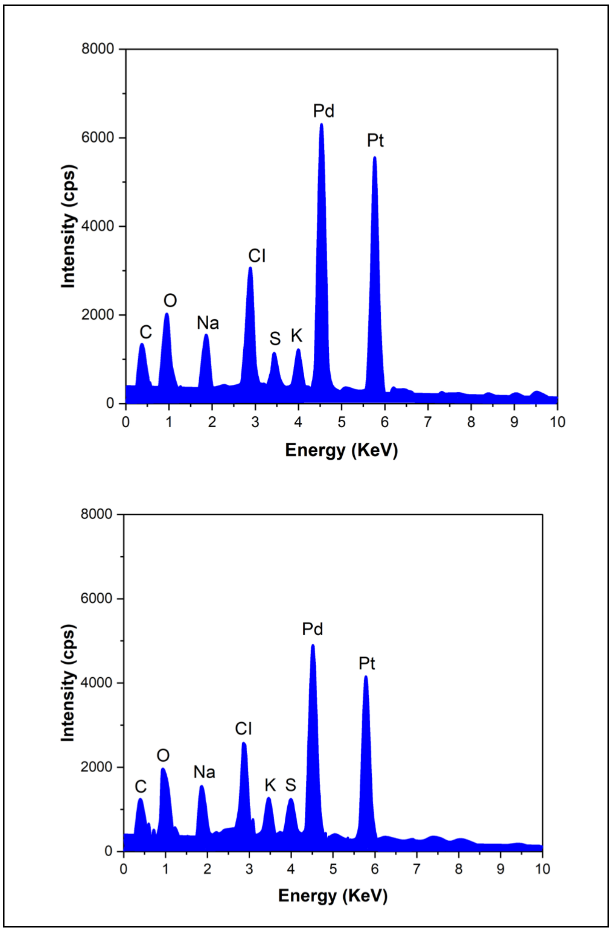

Fig. 7: SEM images and EDX for (a) Untreated hemp fibers, (b) RSE Pd/Pt deposition, (c) RPE Pd/Pt deposition and (d) RPE/RSE Pd/Pt

EDX evaluation were conducted on identical samples, corroborating inclusion of Pt and Pd at treated fibers. Conversely, untreated hemp utilized as a reference exhibited solely carbon and oxygen signals, indicative of the cellulose structure. Distinct Pd and Pt peaks were identified in the Pd/Pt-modified samples, with intensities varying according to the applied extract. The Pd/Pt nanoparticles produced from RPE/RSE exhibited the greatest signal intensities for both elements. Similarly, hemp leaf extract enabled green synthesis of TiO_2 nanoparticles (21–29 nm), with structure confirmed by XRD, FTIR, and composition verified by EDX. The nanoparticles exhibited strong antimicrobial and anticancer activity, demonstrating sustainable nanomaterial development using plant waste (Korkmaz *et al.* 2025).

3.6 Evaluation of Colorimetric Property

Table 4 summarizes the highest-performing from all categories, encompassing RPE and RSE dyeing, combined RPE/RSE treatment and RPE/RSE with nanoparticles.

Table 4. Colorimetric properties of Pd/Pt-treated hemp

Sample	K/S	L*	a*	b*	C*	h°
RPE/Hemp	2.18	68.40	8.25	7.10	10.89	40.72
RSE/Hemp	1.94	66.85	6.40	9.35	11.33	55.61
RPE/RSE/Hemp	2.76	64.90	9.80	8.60	13.04	41.27
RPE/RSE/Pt NPs/Hemp	4.68	59.75	11.60	7.45	13.79	32.72
RPE/RSE/Pd NPs/Hemp	3.85	61.20	10.10	8.05	12.92	38.55
RPE/RSE/Pd/Pt NPs/Hemp	5.42	56.40	12.85	6.90	14.59	28.24

Table 4 illustrates that nanoparticle deposition on dyed fibers results in substantial alterations in color coordinates. The fibers treated with RPE/RSE/Pd/Pt has lowest L* value (56.40), signifying the darkest hue. The reduction at L* due to the presence of Pt and Pd nanoparticles validates increased color intensity. Furthermore, the integration of these nanoparticles decreases the b* value, indicating a reduction in yellowness. This alteration is probably attributable to the structural modification of hydroxyl groups in RPE/RSE, wherein the enol form (–C–OH) transitions to a keto form (–C=O), showing reduction of Pt^{2+} and Pd^{2+} into nanoparticles. Moreover, Pd/Pt ions engage with functional groups in both RPE/RSE and hemp fibers, modifying their chemical environment and causing a change in the fibers' color.

An K/S figure demonstrates significant increase. The comparison of materials dyed with RPE and RSE against those treated with RPE/RSE reveals a distinct improvement. The integration of Pd/Pt nanoparticles into RPE/RSE-dyed fibers elevates K/S value from 2.76 to 5.42, showing significant enhancement at color strength. This enhancement in K/S indicates that Pd/Pt nanoparticles influence the optical behavior of the dyed fibers. Although Pd and Pt exhibit weaker plasmonic effects than Au and Ag nanoparticles, their incorporation can enhance light scattering, modify local electronic interactions, and improve dye–fiber affinity. These effects promote more efficient light absorption and retention of dye molecules, thereby contributing to the increased color strength observed in the treated fabrics. Thus, nanoparticles function as active enhancers of optical performance instead of passive additions. The results demonstrate that the concentration of Pd/Pt ions is crucial in influencing color depth.

3.7 Color Fastness Evaluation

Colorfastness is a crucial characteristic in the choosing of textile dyes, indicating the capacity of materials to withstand fading and maintain their aesthetic quality over time. This feature is crucial for ensuring that dyed textiles retain color stability when exposed to external variables like laundering, light exposure, and abrasion.

The colorfastness outcomes for hemp fibers dyed with RPE/RSE and modified by Pt and Pd nanoparticles under light, rubbing and washing conditions were detailed in Table 5. Fabrics exclusively treated by RPE and RSE showed relatively low resilience to laundering and abrasion. The combination of both extracts (RPE/RSE) resulted in a marginal enhancement in fastness. The incorporation of Pd and Pt nanoparticles into RPE/RSE-treated fabrics resulted in significant improvement at all fastness parameters, with an uplift of roughly 1–2 rating levels. Existing studies reveal that Bridelia micrantha dye achieved optimal absorbance (3.88) and color strength (4.45) using RSM with high model accuracy ($R^2 \approx 0.99$). Dyed leather showed good fastness and antibacterial properties, supporting sustainable natural dye applications (Kalangali *et al.* 2025). Furthermore, the colorfastness evaluations were repeated under identical testing conditions, and consistent ratings were obtained across repeated assessments, confirming the reproducibility and reliability of the observed fastness improvements following Pd/Pt nanoparticle treatment.

Table 5. Color fastness of Pd/Pt-treated hemp

Sample	Light Stability	Washing Durability			Abrasion Fastness	
		Shade Variation	Color Transfer on Hemp	Color Transfer on Wool	Dry	Wet
RPE	5-7	7	7	7	2-7	7
RSE	6	6	6	2-6	6	2-6
RPE / RSE	7	3-7	7	7	3-7	7
RPE / RSE /Pt NPs	7	5	5	5	5	5
RPE / RSE /Pd NPs	6	4	4-5	4	4-5	4
RPE / RSE /Pd/Pt NPs	7-9	4-9	9	9	9	4-9

Among all samples, cloth treated with RPE/RSE/Pd/Pt nanoparticles had the highest stability, demonstrating rubbing fastness and exceptional light fastness along with maximum ratings. The enhancement in light fastness is primarily due to the oxidative stability of dye molecules, rather than the interactions between the dye and fiber. The improved performance outcome from several factors: (1) lowered surface adsorption, (2) intensified interaction among RPE/RSE components and hemp fibers provided Pd/Pt ions, and (3) the establishment of coordination complexes among dye molecules, cellulose fibers and metal ions.

3.8 Evaluation of Antibacterial Property

Table 6 summarizes the antibacterial performance of hemp fibers treated with RPE, RSE, their combination, and subsequent incorporation of Pd and Pt nanoparticles. The untreated fibers exhibited no antibacterial activity, whereas fabrics treated with individual extracts demonstrated moderate inhibition with zones of 8–9 mm for RPE and 7–8 mm for RSE. A synergistic enhancement was observed for the combined RPE/RSE treatment, providing inhibition zones of 11 mm against *S. aureus* and 10 mm attributed to the collective action of bioactive phytochemicals such as phenolics, tannins and flavonoids. According to a past analysis, Equisetum hyemale extracts rich in phenolics and bioactive compounds showed strong antibacterial activity against *S. aureus* and *E. coli*, with enhanced wound healing performance. Optimized extraction improved phenolic content, reducing wound width significantly and promoting faster tissue regeneration (Sivri *et al.* 2026).

The incorporation of Pt nanoparticles further improved antibacterial efficacy, increasing inhibition zones to 14 mm and 15 mm, respectively. Notably, the combined Pd/Pt nanoparticle system exhibited the highest antibacterial efficiency, with inhibition zones 20 mm for *S. aureus* and 18 mm for *E. coli*. This improved activity is primarily associated with the synergistic interaction between Pd and Pt nanoparticles, which facilitates disruption of bacterial cell membranes and induces oxidative stress through catalytic reactive oxygen species generation, thereby leading to effective bacterial inactivation. The enhanced antibacterial activity of the Pd/Pt-functionalized hemp fabrics can also be attributed to the high surface reactivity of the bimetallic nanoparticles, which promotes direct interaction with bacterial cell walls and membranes. Such interactions may alter membrane permeability, induce leakage of intracellular constituents, and interfere with essential cellular functions, ultimately resulting in bacterial inactivation. The superior inhibition zones observed for the Pd/Pt-treated fabrics (20 mm against *S. aureus* and 18 mm against *E. coli*) demonstrate the effectiveness of the bimetallic system compared with plant-extract-treated samples. These values are comparable to or higher than those reported for several natural-dye-based antibacterial textiles and plant-mediated nanoparticle-functionalized fabrics, highlighting the potential of the developed hemp textiles for durable and sustainable antimicrobial applications. Furthermore, antibacterial evaluations were conducted under identical testing conditions, and consistent inhibition zone measurements were obtained across repeated assessments, confirming the reliability and reproducibility of the observed antibacterial performance.

Table 6. Antibacterial activity of Pd/Pt-treated hemp fibers

Sample	*E. coli* Zone of Inhibition (mm)	*S. aureus* Zone of Inhibition (mm)
Untreated hemp fabric	0	0
Hemp + RPE	8	9
Hemp + RSE	7	8
Hemp + RPE + RSE	10	11
Hemp + RPE + RSE + Pt	14	15
Hemp + RPE + RSE + Pt + Pd	18	20

Table 7 illustrates the retention of Pd and Pt nanoparticles on RPE/RSE-treated hemp fibers after repeated washing cycles, along with the corresponding antibacterial performance. The initial concentrations of Pd (120 ppm) and Pt (135 ppm) exhibited high antibacterial reductions exceeding 94% against *S. aureus* and *E. coli*. After 5 washing cycles, nanoparticle content moderately decreased to 102 ppm (Pd) and 118 ppm (Pt), with a slight reduction in antibacterial efficacy, while after 10 cycles, the residual concentrations further declined to 85 ppm and 96 ppm, respectively, still maintaining considerable bacterial reduction efficiencies in the range of 80–86%. This gradual decrease indicates minor leaching; however, the substantial retention confirms strong nanoparticle adhesion facilitated by phytochemical interactions during RPE/RSE-mediated synthesis. The sustained antibacterial activity even after repeated laundering demonstrates the durability and stability of the functionalized fibers. Moreover, the green synthesis approach ensures environmentally friendly processing and biocompatibility, while the integration of ANN–GA optimization contributes to improved nanoparticle binding and consistent antibacterial performance.

Table 7. Pd/Pt retention after washing

Washing Cycles	Pd Content (ppm)	Pt Content (ppm)	*E. coli* Reduction % (Pd)	*E. coli* Reduction % (Pt)	*S. aureus* Reduction % (Pd)	*S. aureus* Reduction % (Pt)
0	120	135	94	96	95	97
5	102	118	88	91	89	92
10	85	96	80	84	82	86

4. CONCLUSION

In this study, a sustainable strategy for the functionalization of hemp fibers was successfully developed through the green synthesis of Pd/Pt nanoparticles using rose-derived extracts. The microwave-assisted process enabled efficient nanoparticle formation with an average particle size of 14.8 nm and a uniform distribution on the fiber surface. The Ridge-regularized RSM model effectively described the relationship between process parameters and color strength, achieving a high training coefficient of determination ($R^2 = 0.9951$) with low prediction errors (RMSE = 0.0629). However, the LOOCV result ($R^2 = 0.6681$) suggests moderate predictive capability under unseen conditions, indicating that further validation using larger datasets would be beneficial. The optimized parameters (1.50 g RPE, 1.50 g RSE, 2.00 mM Pt, and 2.00 mM Pd) yielded a predicted K/S value of 6.6563. Experimental validation demonstrated substantial improvement at color strength, with K/S increasing to 5.42 for Pd/Pt-treated fibers, along with enhanced color fastness ratings (up to 7–9). Furthermore, the treated fibers exhibited strong antibacterial performance, with inhibition zones of 20 mm (*S. aureus*) and 18 mm (*E. coli*), and bacterial reduction efficiencies exceeding 94% in initial conditions. Overall, the results confirm that Pd/Pt nanoparticle incorporation significantly enhances both functional and aesthetic properties of hemp fibers. This study provides a promising and eco-friendly approach for the development of advanced multifunctional textile materials, with potential for further optimization and industrial-scale validation. Despite the promising results, the study is limited by the relatively small experimental dataset and laboratory-scale validation. Future work should focus on large-scale process validation, long-term durability assessment, and comprehensive evaluation of nanoparticle retention and performance under real textile service conditions.

FUNDING

This research received no specific grant from any funding agency in the public, commercial, or not-for-profit sectors.

CONFLICTS OF INTEREST

The authors declare that there is no conflict of interest.

REFERENCES

Agrawal, A., Textile Application of Natural Dye Extracted from Myrobalan (Terminalia chebula): Process Optimisation using RSM, *J. Tex. Assoc.*, 86(2), 221–229 (2025). https://doi.org/10.63665/jta.v86i2.14

Aras, O., Atas, E. and Kazanci, M., Self-Reinforced Cellulosic Nanocomposites: Processing Optimization and Interface Characterization of Hemp Cellulose Matrix Reinforced with Cellulose Nanocrystals, *Polym. Adv. Technol.*, 36(11), e70410(2025). https://doi.org/10.1002/pat.70410

Bazanov, A. V., Prusov, A. N., Prusova, S. M. and Radugin, M. V., Synthesis and properties of graphene-like porous carbon from modified cellulose, *Fullerenes Nanotubes Carbon Nanostruc.*, 33(4), 415–429 (2025). https://doi.org/10.1080/1536383X.2024.2413371

Chitichotpanya, P., Vuthiganond, N., Chutasen, P. and Chitichotpanya, C., In Situ Green Production of Silver Nanoparticles Utilizing Purple Corn Silk Extract for Multifunctional Healthcare Hemp Textiles, *J. Curr. Sci. Technol.*, 16(1), 154(2026). https://doi.org/10.59796/jcst.V16N1.2026.154

Csakvari, A. C., Moisa, C., Radu, D. G., Olariu, L. M., Lupitu, A. I., Panda, A. O., Pop, G., Chambre, D., Socoliuc, V., Copolovici, L. and Copolovici, D. M., Green synthesis, characterization, and antibacterial properties of silver nanoparticles obtained by using diverse varieties of cannabis sativa leaf extracts, *Mol.,* 26(13), 4041(2021). https://doi.org/10.3390/molecules26134041

Dabirifar, Z., Khadempir, S., Kardan, A. and Karaman, C., Boosting the electrocatalytic activity of ZrO_2/MWCNT supported PdPt bi-metallic electrocatalyst towards ethanol oxidation reaction by electrochemical activation process and modeling by artificial neural network approach, *Chem. Eng. Res. Des.*, 180, 38–49(2022). https://doi.org/10.1016/j.cherd.2022.02.009

Eren, S., Öztürk, M., Özenç, A. A. and Eren, H. A., Optimization of Hemp Fabric Natural Dyeing in Supercritical Carbon Dioxide Medium by Response Surface Methodology, *Cellulose Chem. Technol.*, 59(7–8), 929–938(2025). https://doi.org/10.35812/CelluloseChemTechnol.2025.59.78

Haji, A. and Payvandy, P., Application of ANN and ANFIS in prediction of color strength of plasma-treated wool yarns dyed with a natural colorant, *Pig. Resin Technol.*, 49(3), 171–180(2020). https://doi.org/10.1108/PRT-10-2019-0089

Haji, A., Vadood, M., Öztürk, M., Yigit, İ., Eren, S. and Eren, H. A., Prediction of colour strength in environmentally-friendly dyeing of polyester fabric with madder using supercritical carbon dioxide, *Color. Technol.*, 141(1), 44–53 (2025). https://doi.org/10.1111/cote.12757

Haque, A. N. M. A., Zhang, Y., Bayattork, M. and Naebe, M., Green disassembly: direct preparation of cellulose micronised powder from hemp by deep eutectic solvent, Cellulose, 33(1), 175–188 (2026). https://doi.org/10.1007/s10570-025-06887-z

Haskan, N., Kutluay, S. and Şahin, Ö., Green synthesis of copper oxide/nanographene nanocomposite as a novel adsorbent for enhanced CO_2 capture, *Int. J. Phytoremed.*, 27(14), 2132–2143(2025). https://doi.org/10.1080/15226514.2025.2566933

Hossain, S. M. Z., Machine Learning Approaches for Predicting Microplastic Removal, *Arab. J. Sci. Eng.*, 50(13), 10219–10232(2025). https://doi.org/10.1007/s13369-025-10116-x

Kalangali, V. H., China, C. R., Kanth, S. V and Njau, K. N., Optimizing Natural Dye Extraction from the Bark of Bridelia micrantha for Dyeing Vegetable-Tanned Leather Using Statistical Modeling, *Fib. Polym.*, 26(11), 4917–4931(2025). https://doi.org/10.1007/s12221-025-01126-5

Kaur, M., Tewatia, P., Rattan, G., Singhal, S. and Kaushik, A., Diamidoximated cellulosic bioadsorbents from hemp stalks for elimination of uranium (VI) and textile waste in aqueous systems, *J. Hazard. Mater.*, 417, 126060(2021). https://doi.org/10.1016/j.jhazmat.2021.126060

Klaykruayat, B., Pisitsak, P., Chitichotpanya, P. and Klanthip, R., In Situ Synthesis of ZnO Nanoparticles Using Soy Protein Isolate for Sustainable and Multifunctional Finishing of Hemp Fabrics, *Polym.*, 18(1), 116(2026). https://doi.org/10.3390/polym18010116

Klaykruayat, B., Vuthiganond, N. and Chitichotpanya, P., Optimization of ultrasound-assisted anthocyanin extraction from agricultural waste purple corn silk for multifunctional hemp finishes, *J. Met. Mater. Minerals,* 34(4), 2027(2024). https://doi.org/10.55713/JMMM.V34I4.2027

Korkmaz, N., Ceylan, Y., Kısa, D., Güçlü, E., Şen, F. and Karadağ, A., Environmentally friendly synthesis and biological activity assessment of titanium dioxide nanoparticles with hemp (Cannabis sativa L.) leaf extract, *Next Mater.,* 9, 101323 (2025). https://doi.org/10.1016/j.nxmate.2025.101323

Malebo, N. J., Manduna, I. T., Mawunu, M., Chokwe, R. C. and Tlhapi, B., Identification of Antioxidant, Antimicrobial, and Cytotoxic Compounds From Hymenocardia acida Tul. Using Ultra-High-Performance Liquid Chromatography-Quadrupole Exactive-Orbitrap-Mass Spectrometry and Molecular Networking Approach, *Chem. Biodivers.,* 23(2), e02485 (2026). https://doi.org/10.1002/cbdv.202502485

Nayak, C., Loganathan, D., Saravanan, K. and Bhatlu M, L. D., Valorisation of PKM-2 Moringa oleifera leaves waste for adsorption of Titan Yellow dye from aqueous solution, modelling with RSM and ANN, *Biomass Convers. Biorefine.*, 15(16), 22919–22939(2025). https://doi.org/10.1007/s13399-025-06767-3

Orero, B., Ntuli, F., Zvinowanda, C., Sithole, T. and Mashifana, T., Sustainable synthesis of activated carbon from water hyacinth via one-step carbonization-H_3PO_4 activation: Optimization and modeling via RSM-artificial intelligence approach, *Next Mater.,* 9, 101140(2025). https://doi.org/10.1016/j.nxmate.2025.101140

Özgüven, A., Kaya, Z., Özgüven, Ö. F. and Öztürk, D., Modelling and optimization of RSM and ANN techniques in treatment of real textile wastewater using Mn-doped Fe_3O_4/zeolite as heterogeneous catalyst, *Chem. Eng. Res. Des.*, 224, 193–208 (2025). https://doi.org/10.1016/j.cherd.2025.11.012

Patel, P., Gupta, S., Hooda, S. and Mondal, P., Optimization and Modeling of Adsorptive Greywater Treatment System using RSM and ANN, *Water, Air, Soil Pollut.,* 237(3), 189(2026). https://doi.org/10.1007/s11270-025-08817-y

Rakphong, J., Suchaiya, V., Aumnate, C. and Aht-Ong, D., Sustainable Valorization of Hemp Lignin via Deep Eutectic Solvent Extraction and Amination for Enhanced Heavy Metal Adsorption and Advanced Wastewater Treatment Applications, *J. Polym. Environ.,* 33(10), 4411–4429(2025). https://doi.org/10.1007/s10924-025-03656-8

Sadeghi-Kiakhani, M., Hashemi, E. and Norouzi, M. M., Characterization and antibacterial studies of phytosynthesized palladium nanoparticles on wool fibers using colorants extracted from saffron petals, *Int. J. Environ. Sci. Technol.*, 22(3), 1523–1536 (2025a). https://doi.org/10.1007/s13762-024-05758-7

Sadeghi-Kiakhani, M., Hashemi, E. and Norouzi, M. M., Valorization of pistachio (Pistacia vera L.) peel extract as an agricultural waste for green fabrication of bio-silver nanoparticles on cellulosic fabrics, *Indus. Crops Prod.,* 223, 120139(2025b). https://doi.org/10.1016/j.indcrop.2024.120139

Safi, M. and Amirshahi, S. H., Estimation of dye concentration by using Kubelka–Munk and Allen–Goldfinger reflective models: comparing the performance, *Sci. Rep.,* 13(1), 2019(2023). https://doi.org/10.1038/s41598-023-29264-x

Sasunthon, N., Laksee, S. and Pisitsak, P., Preparation of Hemp Fabrics With Durable UV-Protective and Antibacterial Properties Using Silver Nanoparticles, *J. Nanotechnol*., 2025(1), 9695944(2025). https://doi.org/10.1155/jnt/9695944

Shahmoradi, G. F., Razbin, M., Tehrani, M., Zolfipour Aghdam, V. L. and Sadrjahani, M., Modeling and optimization of dyeing process of polyamide 6 and woolen fabrics with plum-tree leaves using artificial intelligence, *Sci. Rep.,* 14(1), 15067(2024). https://doi.org/10.1038/s41598-024-64761-7

Shokrzadeh, S., Razbin, M., Ghaheh, F. S., Tehrani, M. and Sadrjahani, M., Optimizing the eco-friendly dyeing of wool and nylon fabrics with Prangos ferulacea (L.) Lindl using artificial intelligence, *Sci. Rep.,* 15(1), 13267(2025). https://doi.org/10.1038/s41598-025-97551-w

Sivri, F. M., Akkoç, S., Önem, E. and Arın, U. E., Effects of extraction conditions on phenolics content and biological activity of Equisetum hyemale, *Int. J. Secondary Metabolite*, 13(1), 221–230 (2026). https://doi.org/10.21448/ijsm.1651992

Thomas, P., Rumjit, N. P., Lai, C. W. and Bin Johan, M. R., EDTA functionalised cocoa pod carbon encapsulated SPIONs via green synthesis route to ameliorate textile dyes - Kinetics, isotherms, central composite design and artificial neural network, *Sustainable Chem. Pharma*., 19, 100349(2021). https://doi.org/10.1016/j.scp.2020.100349

ul-Ain, M., Abd-ur-Rehman, H. M., Khoja, A. H., Naeem, R., Khan, A. A., Gul, J., Kanwal, H., Kamboh, A. H., Ud Din, I. and Shakir, S., Enhancing Cr (VI) remediation efficiency using hemp-derived biochar: insights into RSM optimization and adsorption kinetics using ANN modelling, *Int. J. Environ. Sci. Technol.,* 22(15), 15189–15210(2025). https://doi.org/10.1007/s13762-025-06612-0

Wu, J., Wang, Y., Zhang, Z., Lu, X., Wang, C., Zhong, Z., Qian, D. and Zhang, T., Optimization of pretreating poplar wood shavings with cellulase to produce binderless fiberboard using response surface methodology, BioResources, 15(3), 6431–6441 (2020). https://doi.org/10.15376/biores.15.3.6431-6441

Zhu, X., Zeng, B., Tang, W., Liu, Q., Yu, Z., Cui, Y. and Wang, J., Natural dye modified hemp fibrous foam for colorimetric NH_3 sensing, *Indus. Crops Prod.,* 191, 115950(2023). https://doi.org/10.1016/j.indcrop.2022.115950